# GEOMETRIC NONLINEAR ANALYSIS OF MECHANICAL PROBLEM UNDER PLANE CONDITIONS BY FEM

**Marko Rupert**

rupert.marko@gmail.com

Programa de Pós Graduação em Engenharia Civil, Universidade Federal de Ouro Preto

Campus Universitário, Morro do Cruzeiro, 35400-000, Ouro Preto, MG, Brasil

**Christianne L. Nogueira**

chris@em.ufop.br

Programa de Pós Graduação em Engenharia Mineral, Universidade Federal de Ouro Preto

Campus Universitário, Morro do Cruzeiro, 35400-000, Ouro Preto, MG, Brasil

**Ricardo A. M. Silveira**

ramsilveira@yahoo.com.br

Programa de Pós Graduação em Engenharia Civil, Universidade Federal de Ouro Preto

Campus Universitário, Morro do Cruzeiro, 35400-000, Ouro Preto, MG, Brasil

***Abstract.*** *This paper presents a generalized, displacement based, formulation of the finite element method for geometric nonlinear analysis of mechanical problem under plane strain and plane stress conditions by using the Total Lagrangian approach and physical linearity of the material. Classical examples under plane stress condition, as cantilever beam and L-beam, are presented and good agreements are observed between the analytical and numerical results. Geotechnical problem under plane strain condition, as the embankment problem subject to self-weight force, is analyzed and comparison between the geometric linear and nonlinear formulations highlights the importance of the nonlinear formulation for high height fills.*

***Keywords:*** *geometrical nonlinear analysis, finite elements methods, Total Lagrangian approach, linear elastic material*



Proceedings of the XXXVIII Iberian Latin-American Congress on Computational Methods in Engineering
P.O. Faria, R.H. Lopez, L.F.F. Miguel, W.J.S. Gomes, M. Noronha (Editores), ABMEC, Florianópolis, SC, Brazil, November 5-8, 2017.

# 1 INTRODUCTION

Civil engineering area can be divided into various branches and one of them is the geotechnical engineering. In the geotechnical engineering branch various problems can be observed, such as foundation, earth retaining walls, and anchor systems, reinforcement of soil, slope stability, embankment construction and excavation. The solution of those problems is not easy to reach and their cost and further influence in constructing structure is significant. Engineers and researchers have been employing a huge effort in the tentative to find a more realistic approach to analyze the geotechnical behavior by including aspects such as material nonlinearity, large deformations, time dependent behavior and changes of boundary conditions.

Analytical solutions are not always easy to obtain. In the beginning of 50’s and 60’s years begun the development of computational mechanics applied to the aerospace engineering. After that, the use of computational mechanics spread to other engineering fields such as geotechnical engineering area.

Filling is a very common problem in geotechnical engineering. During the filling process of mine waste dump, tailing storage, embankment or dam on soft soil, large deformations is observed in deeper layers and in the body of the landfill (Moormann *et al*. (2015) and Mohammadi and Taiebat (2013)).

Analyzing the equilibrium of structures which suffers large displacements by considering a linear physics and geometrical model may not adequately represent true response. When the displacements and rotations of structure are large, it is necessary to include effects of geometry. Considering geometric nonlinearities, strains are not linear functions of displacement. Bathe (1996) divided geometrical nonlinear problems in two categories: a) large displacement, large rotations, but small strains; and, b) large displacement, large rotations and large strains. He proposed Total Lagrangian and Updated Lagrangian approach in order to describe the movement of the body. Other authors such as: Cristfield (1991), Cook (2002), Zienkiewitz (2000) and Belytschko (2014), describe the same approaches. In this work we will consider geometric nonlinearities and linear elastic material.

The nonlinear geometric and linear physics approach of mechanical problem on static equilibrium was adopted in this work and the Lagrangian displacement based finite element formulation is presented and the characteristics matrices are implemented into ANLOG (Análise não linear de obras geotécnicas). The ANLOG is an open code computational program, written in FORTRAN which has been developing by many authors (Zornberg 1989; Nogueira 1992 e 1998; Machado Jr. 2000; Pereira 2003; Pinto 2004; Silva 2005; Oliveira 2006; Yang 2009; Valverde 2010; Armond and Nogueira 2013; Simão 2014; Rupert 2017).

# 2 GEOMETRIC NONLINEAR FORMULATION

Consider a deformable continuum body with ${}^0V$ volume and ${}^0S$ contour at initial configuration as depicted in Figure 1. Now, consider a generic ${}^0p$ particle body on the initial configuration at the position ${}^0\mathbf{x}$ related to a stationary coordinate system xyz. During a deformation process, the body particles will experience large displacement and so its configuration will change on each generic instant t (${}^tV$ volume and ${}^tS$ contour).

By adopting a total Lagrangian formulation, which considers the initial configuration as a referential configuration, the position of a generic particle body in any configuration at t and t+Δt can be obtained by adopting an incremental approach as follows:

$$ {}^{t}\mathbf{x} = {}^{0}\mathbf{x} + {}^{t}\mathbf{u} \tag{1}$$

$$ {}^{t+\Delta t}\mathbf{x} = {}^{0}\mathbf{x} + {}^{t+\Delta t}\mathbf{u} \tag{2}$$

where ${}^{0}\mathbf{x}$ is the initial position vector of the body particle p; ${}^{t}\mathbf{x}$ and ${}^{t}\mathbf{u}$ are the position and the displacement vectors of the body particle p at configuration t; and, ${}^{t+\Delta t}\mathbf{x}$ and ${}^{t+\Delta t}\mathbf{u}$ are the position and the displacement vectors of the body particle p at configuration t+Δt.

In a generic configuration t, the varition position of a generic particle body, can be expressed by the deformation gradient tensor (**F**) defined as:

$$ {}_{0}^{t}\mathbf{F} = \left[ {}_{0}\nabla \, {}^{t}\mathbf{x}^{T} \right]^{T} \tag{3}$$

where ${}_{0}\nabla$ is vector differential opetaror.

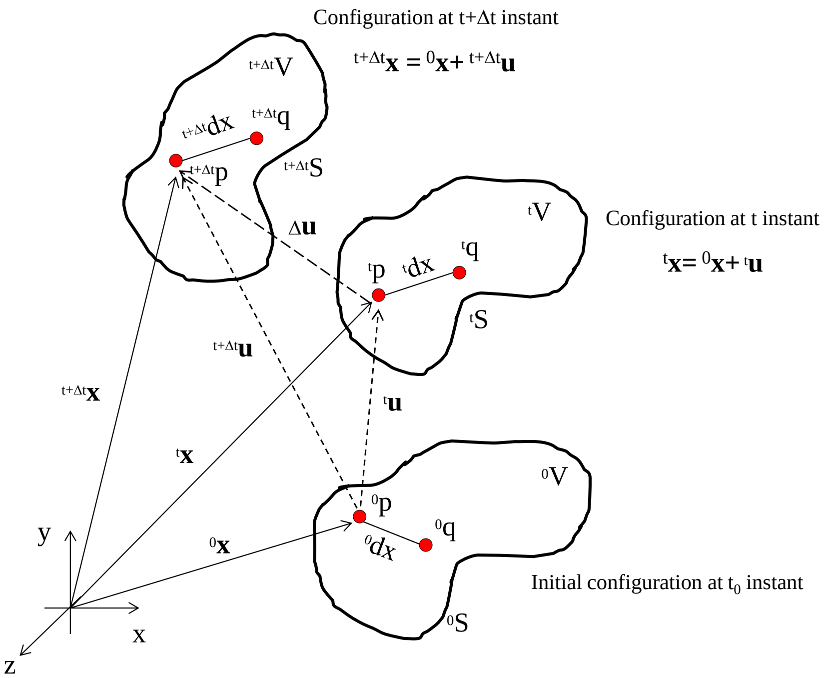


**Figure 1 - Deformable continuum body movement**

By using the deformation gradient tensor, it is possible to obtain the diferential lenght (d**x)** and the diferential volume (dV) in any configuration t by doing:

$$ {}^{t}d\mathbf{x} = {}_{0}^{t}\mathbf{F}\, {}^{0}d\mathbf{x} \tag{4}$$

$$ {}^{t}dV = \det({}_{0}^{t}\mathbf{F})\, {}^{0}dV \tag{5}$$

It is important to state that, during the deformation process the mass of the body is kept constant. So, it is possible to demonstrate that:

$$\int_{{}^{t}V} {}^{t}\rho \, d\,{}^{t}V = \int_{{}^{0}V} {}^{0}\rho \, d\,{}^{0}V \tag{6a}$$

or

$${}^{t}\rho = \frac{1}{\det({}_{0}^{t}\mathbf{F})}\,{}^{0}\rho \tag{6b}$$

When considering large displacement, attention must be given to the strain and stress measurement. The deformation gradient tensor is non-null tensor even during a rigid-body motion. Therefore, it is not the true measures of the body strain. The suitable measure of the body straining, in an incremental total Lagrangian formulation is represented by the Green-Lagrange tensor (**ε)** which considers the change in the squares of length vectors (d**x)** between the undeformed and deformed configuration t. In any deformed configuration at t, this tensor is defined by (considering the signal convention of compression positive):

$${}_{0}^{t}\boldsymbol{\varepsilon} = -\frac{1}{2}\left({}_{0}^{t}\mathbf{F}^{T}\,{}_{0}^{t}\mathbf{F} - \mathbf{I}\right) \tag{7}$$

where **I** is the identity matrix.

In terms of stress, it is important to state which area (at initial or deformed configuration), is considered as reference. The symmetric Cauchy tensor (**σ)** is defined as the real stress measurement since it relates the force vector (**t)** with the differential area dS, with unit normal vector **n**, on a deformed configuration t. So it is possible to state that:

$${}^{t}\mathbf{t}\,d\,{}^{t}S = {}_{t}^{t}\boldsymbol{\sigma}\,{}^{t}\mathbf{n}\,d\,{}^{t}S \tag{8a}$$

or

$${}^{t}\mathbf{t}\,d\,{}^{t}S = {}_{0}^{t}\mathbf{S}\;{}^{0}\mathbf{n}\,{}^{0}dS \tag{8b}$$

or

$${}^{t}\mathbf{t}\,d\,{}^{t}S = {}^{0}\mathbf{t}\,d\,{}^{0}S \tag{8c}$$

where ${}_{0}^{t}\mathbf{S}$ is the second Piola-Kirchhoff stress tensor which is defined as:

$${}_{0}^{t}\mathbf{S} = \det({}_{0}^{t}\mathbf{F})\left({}_{0}^{t}\mathbf{F}\right)\left({}_{t}^{t}\boldsymbol{\sigma}\right)({}_{0}^{t}\mathbf{F})^{-T} \tag{9}$$

## 2.1 Governing differential equation of mechanical problem

Considering the equilibrium of forces in the current deformed configuration it is possible to stablish the following balance equation in terms of the Cauchy stress tensor, **σ** in ${}^{t}V$:

$$\left({}_{t}\nabla^{T}\,{}^{t}\boldsymbol{\sigma}\right)^{T} + {}^{t}\mathbf{b} = \mathbf{0} \tag{10}$$



Proceedings of the XXXVIII Iberian Latin-American Congress on Computational Methods in Engineering
P.O. Faria, R.H. Lopez, L.F.F. Miguel, W.J.S. Gomes, M. Noronha (Editores), ABMEC, Florianópolis, SC, Brazil, November 5-8, 2017.

where **b** is the body force vector and ${}_{t}\nabla$ is the vector differential operator in the position t.

By adopting an incremental approach and a total Lagrangian formulation, it is possible to obtain the equilibrium condition at deformed (and unknown) configuration t+Δt by using the principle of virtual displacement by doing (Bathe, 1992):

$$\int_{{}^{t+\Delta t}V} \left(\delta\, {}^{t+\Delta t}\mathbf{e}\right)^{T}\, {}^{t+\Delta t}\boldsymbol{\sigma}\, d^{t+\Delta t}V = \int_{{}^{t+\Delta t}V} \left(\delta\, {}^{t+\Delta t}\mathbf{u}\right)^{T}\, {}^{t+\Delta t}\mathbf{b}\; d^{t+\Delta t}V + \int_{{}^{t+\Delta t}S_q} \left(\delta\, {}^{t+\Delta t}\mathbf{u}^{s}\right)^{T}\, {}^{t+\Delta t}\mathbf{t}\; d^{t+\Delta t}S_q \tag{11}$$

where **u** is the displacement vector, $\mathbf{u}^s$ is the displacement vector at surface $S_q$, and, **e** is the linear strain tensor. Since the configuration at time t+Δt is unknown it is necessary to refer applied force, stress and strain to a known equilibrium configuration. By adopting the motion of the body related to a fixed (stationary) Cartesian coordinate system, it is possible to obtain the relationship between the Cauchy stress tensor and the linear strain tensor, respectively, with the second Piola Kirchhoff stress tensor and the Green-Lagrange strain tensor by doing:

$${}^{t+\Delta t}\boldsymbol{\sigma} = \frac{{}^{t+\Delta t}\rho}{{}^{0}\rho}\,({}^{t+\Delta t}_{0}\mathbf{F})({}^{t+\Delta t}_{0}\mathbf{S})({}^{t+\Delta t}_{0}\mathbf{F})^{T} \tag{12}$$

$${}^{t+\Delta t}\mathbf{e} = ({}^{0}_{t}\mathbf{F})^{T}({}^{t+\Delta t}_{0}\boldsymbol{\varepsilon})({}^{0}_{t+\Delta t}\mathbf{F}) \tag{13}$$

Using the definitions on Eqs. (5), (6), (8), (12) and (13), the Eq. (11) can be rewritten in terms of the Second Piola Kirchhoff stress tensor and the Green-Lagrange strain tensor as follows:

$$\int_{{}^{0}V} \left(\delta\, {}^{t+\Delta t}_{0}\boldsymbol{\varepsilon}\right)^{T}\, {}^{t+\Delta t}_{0}\mathbf{S}\; d^{0}V = \int_{{}^{0}V} \left(\delta\, {}^{t+\Delta t}\mathbf{u}\right)^{T}\, {}^{0}\mathbf{b}\, d^{0}V + \int_{{}^{0}S_q} \left(\delta\, {}^{t+\Delta t}\mathbf{u}^{s}\right)^{T}\, {}^{0}\mathbf{t}\, d^{0}S_q \tag{14}$$

Considering that the variation, or virtual displacement, occurs at the configuration t, it is possible to states that:

$$\delta\, {}^{t+\Delta t}\mathbf{u} = \delta\left({}^{t}\mathbf{u} + \Delta\mathbf{u}\right) = \delta\Delta\mathbf{u} \tag{15}$$

and

$$\delta\, {}^{t+\Delta t}_{0}\boldsymbol{\varepsilon} = \delta\left({}^{t}_{0}\boldsymbol{\varepsilon} + {}_{0}\Delta\boldsymbol{\varepsilon}\right) = \delta\, {}_{0}\Delta\boldsymbol{\varepsilon} \tag{16}$$

Replacing the Eqs. (15) and (16) into Eq. (14) one can obtain:

$$\int_{{}^{0}V} \left(\delta_{0}\Delta\boldsymbol{\varepsilon}\right)^{T}\, {}^{t+\Delta t}_{0}\mathbf{S}\, d^{0}V = \int_{{}^{0}V} \left(\delta\Delta\mathbf{u}\right)^{T}\, {}^{0}\mathbf{b}\, d^{0}V + \int_{{}^{0}S_q} \left(\delta\Delta\mathbf{u}^{s}\right)^{T}\, {}^{0}\mathbf{t}\; d^{0}S_q \tag{17}$$

The incremental parcel of the Green-Lagrange strain tensor can be divided into two parcels: linear ($\Delta\mathbf{e}$) and nonlinear ($\Delta\boldsymbol{\eta}$) as follows:

$${}_{0}\Delta\boldsymbol{\varepsilon} = -\left({}_{0}\Delta\mathbf{e} + {}_{0}\Delta\boldsymbol{\eta}\right) \tag{18}$$

Where,

$${}_{0}\Delta\mathbf{e} = \frac{1}{2}\left[{}_{0}\nabla\Delta\mathbf{u}^{T}\right]^{T} + \left[{}_{0}\nabla\Delta\mathbf{u}^{T}\right] \tag{19}$$

$$ {}_0\Delta\boldsymbol{\eta} = \frac{1}{2}\left[{}_0\nabla\Delta\mathbf{u}^{\mathrm{T}}\right]^{\mathrm{T}}\left[{}_0\nabla\Delta\mathbf{u}^{\mathrm{T}}\right] \tag{20} $$

Also, considering that the variation occurs at the configuration t, it is possible to obtain the following incremental decomposition:

$$ {}^{t+\Delta t}_{0}\mathbf{S} = {}^{t}_{0}\mathbf{S} + {}_0\Delta\mathbf{S} \tag{21} $$

where, considering the constitutive relationship, one can obtain:

$$ {}_0\Delta\mathbf{S} = {}_0\mathbf{D}\,{}_0\Delta\mathbf{e} \tag{22} $$

Substituting Eqs. (18), (21) and (22) into Eq. (17) one can obtain:

$$ \begin{aligned} &-\int_{{}^0V}\left(\delta_0\Delta\mathbf{e}\right)^{\mathrm{T}}\,{}_0\mathbf{D}\,{}_0\Delta\mathbf{e}\,\mathrm{d}^0V - \int_{{}^0V}\left(\delta_0\Delta\boldsymbol{\eta}\right)^{\mathrm{T}}\,{}^{t}_{0}\mathbf{S}\,\mathrm{d}^0V = \\ &\int_{{}^0V}\left(\delta\Delta\mathbf{u}\right)^{\mathrm{T}}\,{}^0\mathbf{b}\,\mathrm{d}^0V + \int_{{}^0S_q}\left(\delta\Delta\mathbf{u}^{s}\right)^{\mathrm{T}}\,{}^0\mathbf{t}\;\mathrm{d}^0S_q + \int_{{}^0V}\left(\delta_0\Delta\mathbf{e}\right)^{\mathrm{T}}\,{}^{t}_{0}\mathbf{S}\,\mathrm{d}^0V \end{aligned} \tag{23} $$

## 2.2 Finite element method formulation

By using a displacement based formulation of FEM, one can obtain:

$$ \mathbf{u} = \mathbf{N}\hat{\mathbf{u}} \tag{24} $$

where $\mathbf{N}$ is the interpolation function matrix and $\hat{\mathbf{u}}$ is the nodal displacement vector. Using the definition on Eqs. (19) and (20), the incremental, linear strain tensor and the second order strain tensor , can be written as:

$$ {}_0\Delta\mathbf{e} = \left(\mathbf{B}_{L0} + \mathbf{B}_{L1}\right)\Delta\hat{\mathbf{u}} \tag{25} $$

$$ {}_0\Delta\boldsymbol{\eta} = \mathbf{B}_{NL}\Delta\hat{\mathbf{u}} \tag{26} $$

Replacing Eqs. (25) and (26) into the Eq. (23) one can obtain:

$$ \begin{aligned} &\int_{{}^0V}\left(\left(\mathbf{B}_{L0}+\mathbf{B}_{L1}\right)\delta\Delta\hat{\mathbf{u}}\right)^{\mathrm{T}}\,{}_0\mathbf{D}\left(\left(\mathbf{B}_{L0}+\mathbf{B}_{L1}\right)\Delta\hat{\mathbf{u}}\right)\mathrm{d}^0V + \int_{{}^0V}\left(\mathbf{B}_{NL}\delta\Delta\hat{\mathbf{u}}\right)^{\mathrm{T}}\,{}^{t}_{0}\mathbf{S}\left(\mathbf{B}_{NL}\Delta\hat{\mathbf{u}}\right)\mathrm{d}^0V = \\ &-\int_{{}^0V}\left(\left(\mathbf{B}_{L0}+\mathbf{B}_{L1}\right)\delta\Delta\hat{\mathbf{u}}\right)^{\mathrm{T}}\,{}^{t}_{0}\mathbf{S}\,\mathrm{d}^0V - \int_{{}^0V}\left(\mathbf{N}\delta\Delta\hat{\mathbf{u}}\right)^{\mathrm{T}}\,{}^0\mathbf{b}\,\mathrm{d}^0V - \int_{{}^0S_q}\left(\mathbf{N}\delta\Delta\hat{\mathbf{u}}^{s}\right)^{\mathrm{T}}\,{}^0\mathbf{q}\;\mathrm{d}^0S_q \end{aligned} \tag{27} $$

Rearranging the term and considering any non-null virtual incremental displacement vector $(\delta\Delta\mathbf{u})$, one can obtain:

$$ \mathbf{K}\,\Delta\hat{\mathbf{u}} = {}^{t+\Delta t}\mathbf{F}_{ext} - {}^{t}\mathbf{F}_{int} \tag{28} $$

where $\mathbf{K}$ is the stiffness matrix which can be separeted by parts, as follow:

$$ \mathbf{K} = \mathbf{K}_{L1} + \mathbf{K}_{L2} + \mathbf{K}_{L3} + \mathbf{K}_{L4} + \mathbf{K}_{NL} \tag{29} $$

where



Proceedings of the XXXVIII Iberian Latin-American Congress on Computational Methods in Engineering
P.O. Faria, R.H. Lopez, L.F.F. Miguel, W.J.S. Gomes, M. Noronha (Editores), ABMEC, Florianópolis, SC, Brazil, November 5-8, 2017.

$$\mathbf{K}_{L1} = \int_{^0V} \mathbf{B}_{L0}{}^T \, {}_0\mathbf{D} \, \mathbf{B}_{L0} \; d^0V \tag{30}$$

is the linear contribution of the stiffness matrix; :

$$\mathbf{K}_{L2} = \int_{^0V} \mathbf{B}_{L1}{}^T \, {}_0\mathbf{D} \, \mathbf{B}_{L0} \; d^0V \tag{31}$$

$$\mathbf{K}_{L3} = \int_{^0V} \mathbf{B}_{L0}{}^T \, {}_0\mathbf{D} \, \mathbf{B}_{L1} \; d^0V \tag{32}$$

$$\mathbf{K}_{L4} = \int_{^0V} \mathbf{B}_{L1}{}^T \, {}_0\mathbf{D} \, \mathbf{B}_{L1} \; d^0V \tag{33}$$

are the geometrical contributions of the stiffness matrix; :

$$\mathbf{K}_{NL} = \int_{^0V} \mathbf{B}_{NL}{}^T \, {}_0^t\mathbf{S} \, \mathbf{B}_{NL} \; d^0V \tag{34}$$

is the stress state contribution of the stiffness matrix.

The external forces vector at the configuration t+Δt is obtained by doing:

$${}^{t+\Delta t}\mathbf{F}_{ext} = -\,{}^{t+\Delta t}\mathbf{F}_b - {}^{t+\Delta t}\mathbf{F}_q \tag{35}$$

where

$${}^{t+\Delta t}\mathbf{F}_b = \int_{^0V} \mathbf{N}^T \; {}^{t+\Delta t}\mathbf{b} \, d^0V \tag{36}$$

is the nodal force vector equivalent to the body force **b**; and

$${}^{t+\Delta t}\mathbf{F}_q = \int_{^0S_q} \mathbf{N}^T \; {}^{t+\Delta t}\mathbf{t} \; d^0S_q \tag{37}$$

is the nodal force vector equivalent to the surface force **t**.

The internal force is defined as:

$${}^t\mathbf{F}_{int} = \int_{^0V} \left(\mathbf{B}_{L0} + \mathbf{B}_{L1}\right)^T \; {}_0^t\mathbf{S} \, d^0V \tag{38}$$

where ${}_0^t\mathbf{S}$ is the second Piola-Kirchhoff stress tensor.

## 2.3 Incremental-iterative procedures

In the incremental process for the equilibrium path is controlled by the load factor λ, which is updated at the end of each step by doing:

$${}^{t+\Delta t}\lambda = {}^t\lambda + \Delta\lambda \tag{39}$$

where Δλ is the incremental load factor which can be defined by adopting an automatic strategy, as proposed by Ramm (1981, 1982). The incremental load factor is used to obtain the increment of external force by doing:

$$\Delta\mathbf{F}_{ext} = \Delta\lambda\mathbf{F}_{ext} \tag{40}$$

At the end of each step the external force vector, the displacement vector, the linear strain tensor, the Piola-Kirchhoff stress tensor, and the internal force vector are updated, respectively, by doing:

$${}^{t+\Delta t}\mathbf{F}_{ext} = {}^{t}\mathbf{F}_{ext} + \Delta\mathbf{F}_{ext} \tag{41}$$

$${}^{t+\Delta t}\mathbf{U} = {}^{t}\mathbf{U} + \Delta\mathbf{U} \tag{42}$$

$${}^{t+\Delta t}_{0}\mathbf{e} = {}^{t}_{0}\mathbf{e} + {}_{0}\Delta\mathbf{e} \tag{43}$$

$${}^{t+\Delta t}\mathbf{F}_{int} = {}^{t}\mathbf{F}_{int} + \Delta\mathbf{F}_{int} \tag{44}$$

The Cauchy stress tensor, at the end of each step, is obtained by doing:

$${}^{t+\Delta t}\boldsymbol{\sigma} = \frac{{}^{t+\Delta t}\rho}{{}^{0}\rho}\left({}^{t+\Delta t}_{0}\mathbf{F}\right)\left({}^{t+\Delta t}_{0}\mathbf{S}\right)\left({}^{t+\Delta t}_{0}\mathbf{F}\right)^{T} \tag{45}$$

In incremental-iterative process, internal and external forces are balanced through iterative process. The Newton-Raphson method is the most common used technique to solve nonlinear equations. The incremental displacement vector is obtained by doing:

$$\Delta\mathbf{U} = \Delta\mathbf{U}^{0} + \sum_{k=1}^{iter}\delta\Delta\mathbf{U}^{k} \tag{46}$$

where

$$\Delta\mathbf{U}^{0} = {}^{t}_{0}\mathbf{K}^{-1}\Delta\mathbf{F}_{ext} \tag{47}$$

is the predicted incremental displacement vector and,

$$\delta\Delta\hat{\mathbf{U}}^{k} = \mathbf{K}^{-1}\ \boldsymbol{\psi}^{k} \tag{48}$$

is the corrector incremental displacement vector where,

$$\boldsymbol{\psi}^{k} = \left({}^{t+\Delta t}\mathbf{F}_{ext} - {}^{t}\mathbf{F}_{int}{}^{k}\right) \tag{49}$$

is the unbalanced force vector which is calculated at each iteration k. The equilibrium condition is defined according to the convergence criterion adopted. Table 1 presents some convergence criterion that computational program ANLOG can use. The evaluated ratio (Table 1) on each iterative cycle should be smaller than a defined tolerance.

Table 1 - Convergence criteria

| Criteria | ratio |
|---|---|
| Force | $\Vert\mathbf{F}_e - \mathbf{F}_i\Vert / \Vert\mathbf{F}_e\Vert$ |
| Displacement | $\Vert\delta\Delta\mathbf{U}\Vert / \Vert\Delta\mathbf{U}\Vert$ |
| Energy | $\Vert\delta\Delta\mathbf{U}\cdot\boldsymbol{\Psi}\Vert / \Vert\Delta\mathbf{U}^{0}\cdot\Delta\mathbf{F}_e\Vert$ |

# 3 NUMERICAL EXAMPLES

This item presents three mechanical problems: two on plane stress condition and one on plane strain condition. These examples are used to verify the computational implementation introduced into ANLOG system in order to include the geometric nonlinearities effects.

## 3.1 Cantilever beam

In this item a cantilever beam of length L, height h and thickness b (Fig 2) submitted to a vertical load F (which remains in a vertical position even during the deformation path) is analyzed in the context of geometrical nonlinearity but in the context of physical linearity.

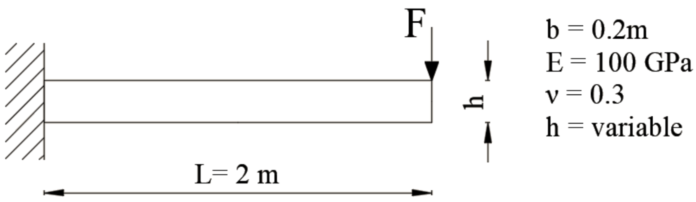


**Figure 2 - Cantilever beam subjected to an end shear force**

The proposed formulation will be tested with Q4 and Q8 quadrilateral element using full Gauss integration 2 by 2, and 3 by 3, respectively. Using modified Newton-Raphson incremental-iterative process, with 100 incremental steps and tolerance of $10^{-5}$. Figure 3 presents the discretization considering 40 elements.

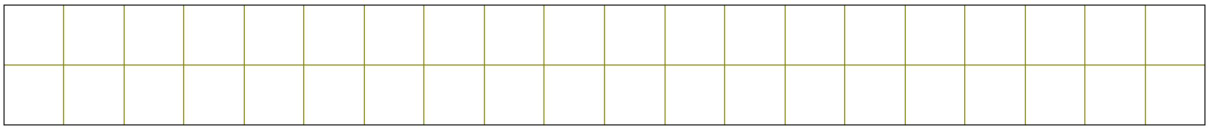

**Figure 3 - Mesh used to modeled beam (h=variables)**

Figures 4 and 5 show the comparison between the numerical results obtained by ANLOG using total Lagrangian formulation and the analytical solution considering geometric nonlinearity and material linear Euler-Bernoulli theory (Timoshenko and Gere, 1991) in terms of the normalized vertical (v/L) and horizontal (u/L) displacement and normalized force ($FL^2/EI$), where I is moment of inertia.

For the beam, h=0.02 and L/h=100, good agreements with analytical results can be observed in Fig. 4. For the beam, h=0.2 and L/h=10, it can be seen on Fig. 5 small shift from analytical results due to shear effect. Small difference on the results can observed due to the element influence (Q4 and Q8 elements). Problems with bigger nonlinearities are better represented when using Q8 elements.

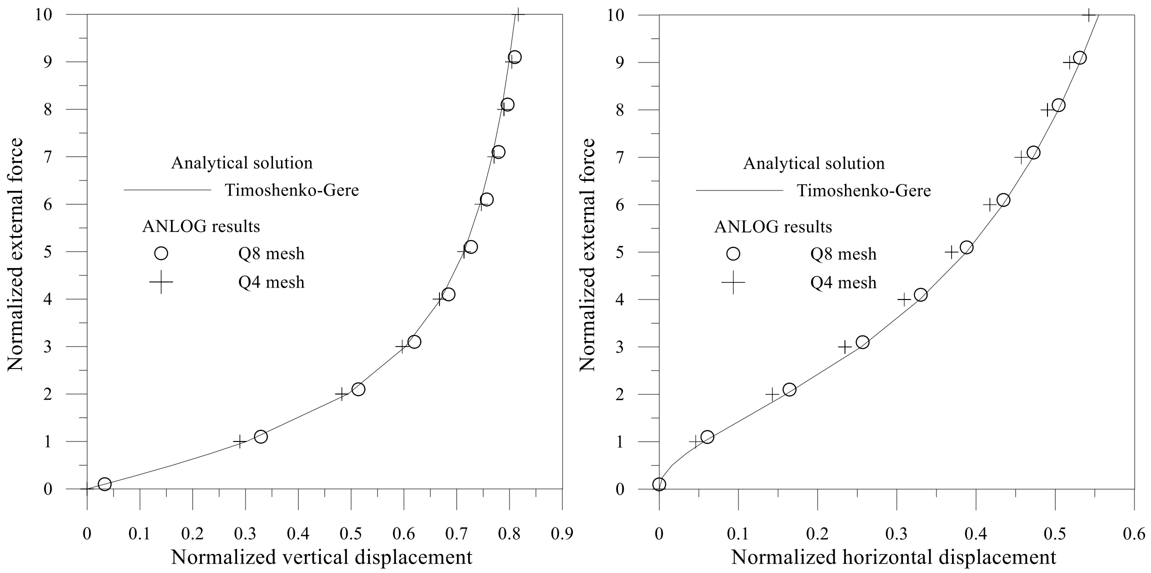


**Figure 4 - ANLOG results mesh with Q4 and Q8 compared with analytical solution for beam h=0.02**

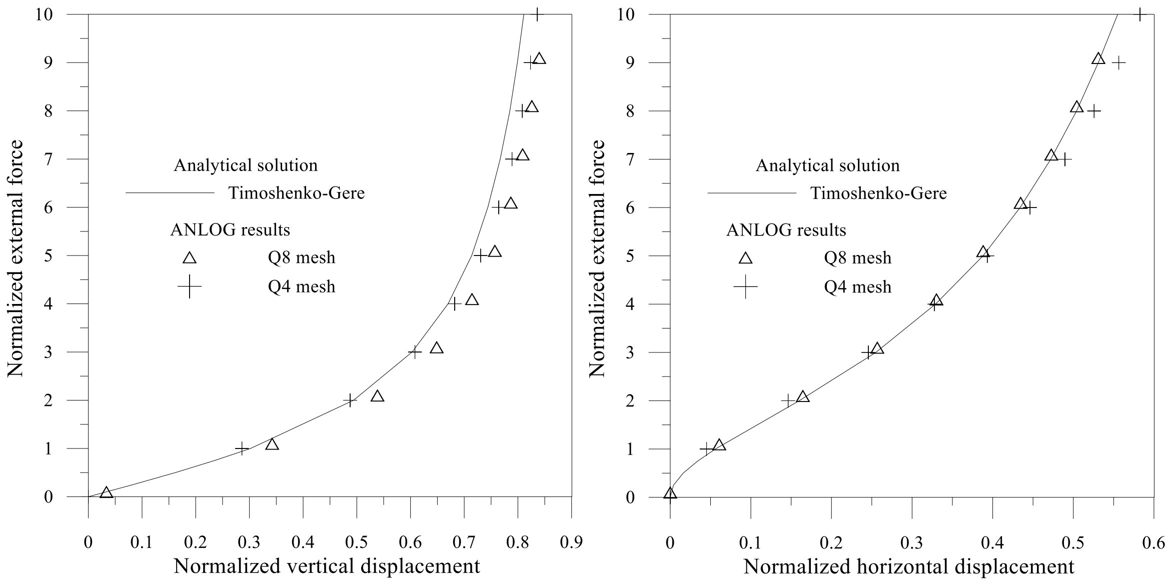


**Figure 5 - ANLOG results mesh with Q4 and Q8 compared with analytical solution for beam h=0.2 m**

## 3.2 L-shaped beam

L-shaped beam, depicted in Fig. 6, with 10 m each part of L shape and as height 1m, is one of the benchmark tests to test large displacement formulations. The analysis is conducted in a plane stress condition considering Young Modulus of 30 MPa and Poisson ration of 0.3. A concentrated horizontal force F of 40 kN is applied at the point A.

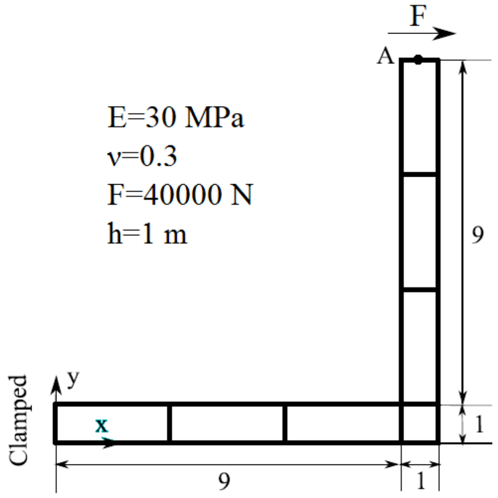


**Figure 6 - L beam under horizontal load**

Figure 7 shows different discretization used. Mesh in Fig 7c was tested with Q4 and Q8 elements while meshes in Fig 7a and 7b were tested only with Q8 elements. During the incremental-iterative process tolerance was set to $10^{-4}$ and incremental process was divided in 100 steps. The convergence criterion was satisfied after 2 or 3 iterations.

Figure 8 presents the results in terms of the horizontal displacement of the point A, provided by Battini (2008) and obtained numerically by ANLOG. Q8 element discretization shows better performance.

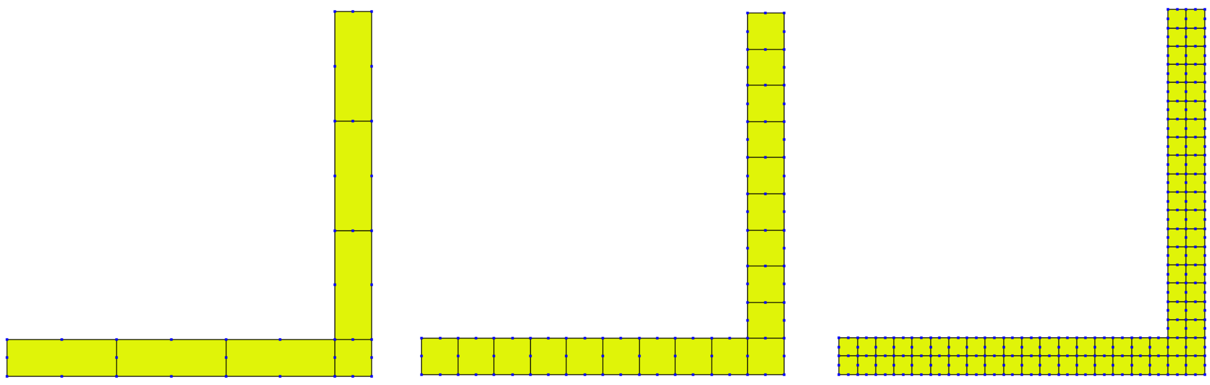

**a) 7 elements** **b) 19 elements** **c) 76 elements**

**Figure 7 - Q8 element mesh used**

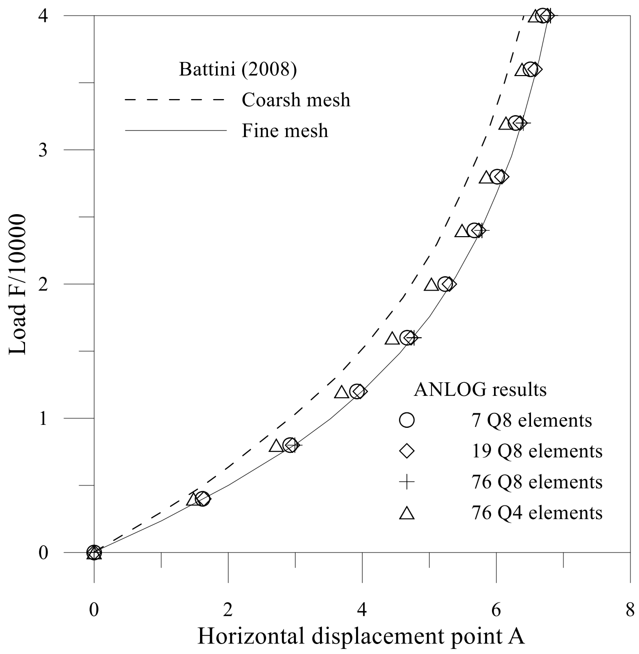


**Figure 8 - Equilibrium path Battini (2008) and ANLOG**

## 3.3 Embankment

In the following example, simple embankment will be studied in plane strain condition. Figure 9 illustrates the symmetric part of the embankment with height (H), half crest length (LC) and half base length (LB). In this figure also are defined some control points: point “a” at middle of the crest; point “b” on the edge of crest; and, point “c” on the bottom and the edge of the embankment. These control points are used to illustrate the movement of the embankments in terms of the normalized horizontal displacement (u/H) and normalized vertical displacement (v/H) by considering different approach: geometric linear and geometric nonlinear. The embankment material is considered as linear elastic with Young Modulus of 10MPa and Poisson ratio of 0.3. The self-weight of the material is adopted as 20kN/m$^3$.

An initial finite element mesh with 100 Q8 elements is used, varying the embankment dimension but keeping constant the relation H/LB/LC from 10/12/2 to 100/120/20. The embankment’s construction process is considered in only one layer of height H. The modified Newton-Raphson incremental-iterative process, with 100 incremental steps and tolerance of $10^{-4}$ was used to obtain nonlinear response of each embankment configuration.

Figure 10 and 11 presents the numerical results in terms of normalized horizontal and vertical displacement in the controls points. As can be seen, there is no difference on the nonlinear and linear displacements for embankment height lower that 40m. As the embankment height increases the difference between the both approaches appears.



Proceedings of the XXXVIII Iberian Latin-American Congress on Computational Methods in Engineering
P.O. Faria, R.H. Lopez, L.F.F. Miguel, W.J.S. Gomes, M. Noronha (Editores), ABMEC, Florianópolis, SC, Brazil, November 5-8, 2017.

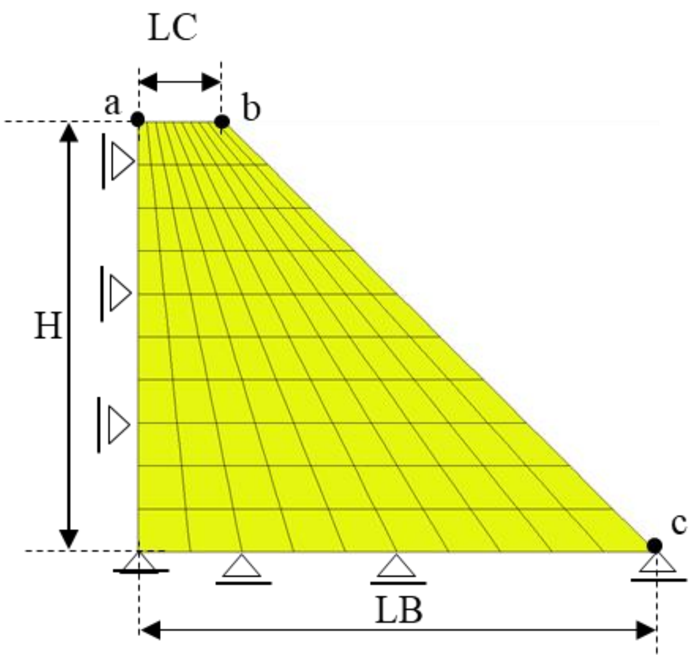


**Figure 9 Embankment on rigid foundation – FEM mesh – 100 Q8 elements**

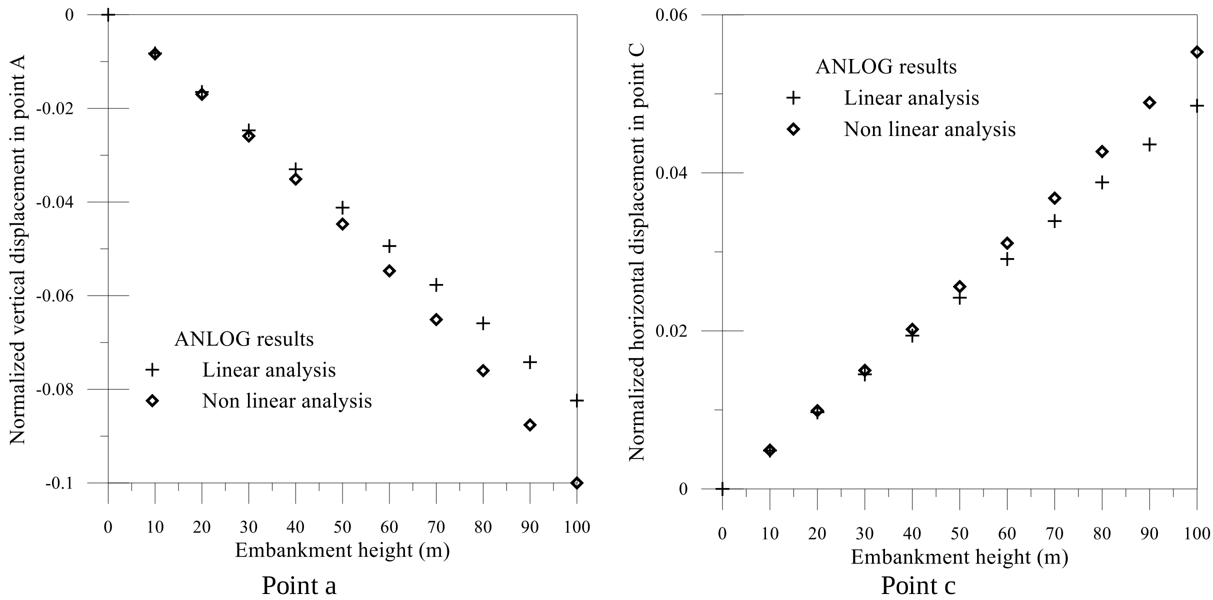


**Figure 10 Numerical embankment's movement at points a and c**



Proceedings of the XXXVIII Iberian Latin-American Congress on Computational Methods in Engineering P.O. Faria, R.H. Lopez, L.F.F. Miguel, W.J.S. Gomes, M. Noronha (Editores), ABMEC, Florianópolis, SC, Brazil, November 5-8, 2017.

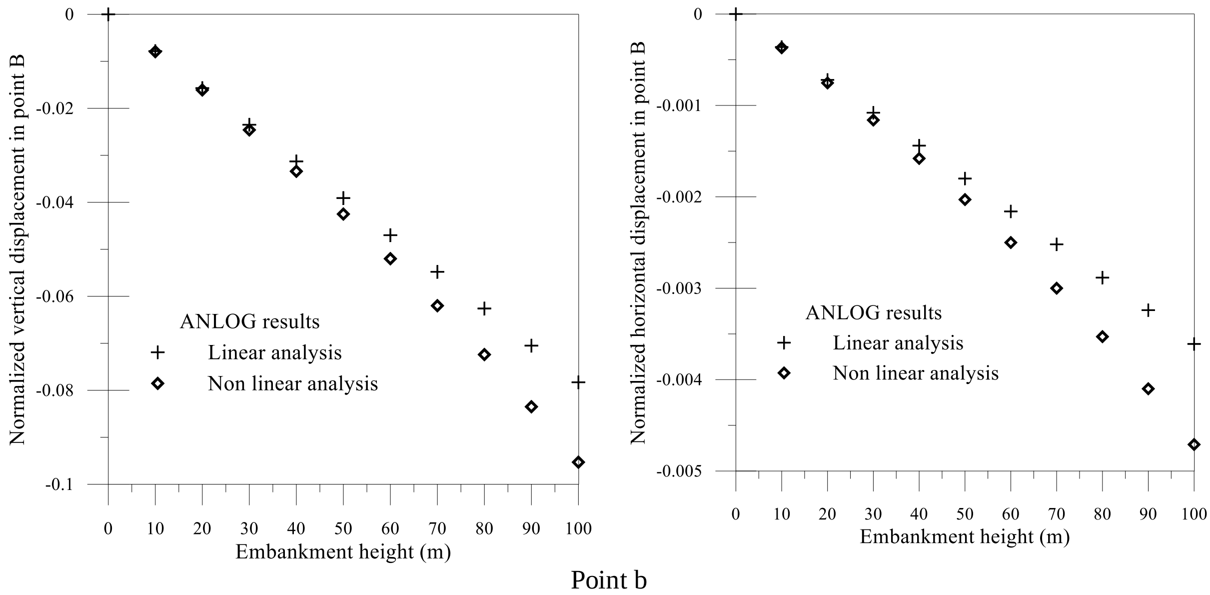


**Figure 11 Numerical embankment's movement at the point b**

To evaluate the influence of the fill process, the embankment with dimension H/LB/LC of 100/120/20 was analyzed by using a refined mesh as depicted on Fig. 12 and considering a construction process of 10 stages of 10m layers. To obtain nonlinear solution modified Newton-Raphson incremental-iterative process was used, with 10 incremental steps per layer and tolerance of $10^{-4}$ was adopted.

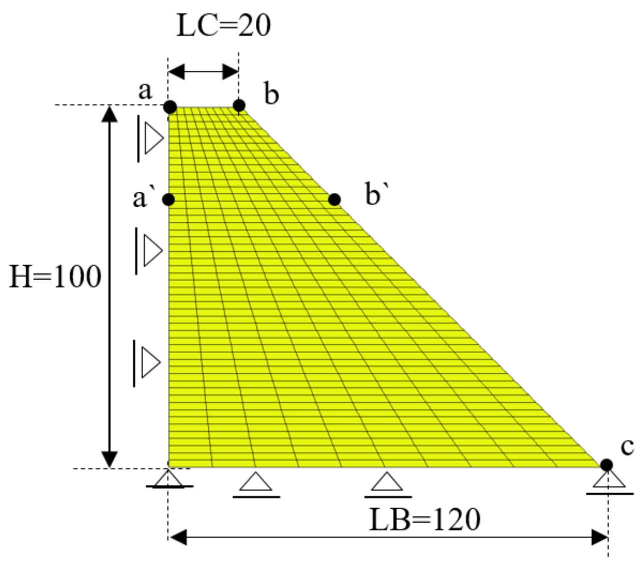


**Figure 12 - Embankment on rigid foundation**

Figure 13 shows the normalized vertical displacements (v/H) throughout the embankment axis at the final fill process. There is no significant difference between the linear and nonlinear analysis for the point on the top of embankment. Greater difference can be shown along the axis in the middle of embankment. Nonlinear analysis shows greater displacements.

Figure 14 shows the horizontal normalized (u/H) displacements during construction in point c, where H is current constructed height. As one can see, the nonlinear and linear responses diverge for height higher than 40 m.

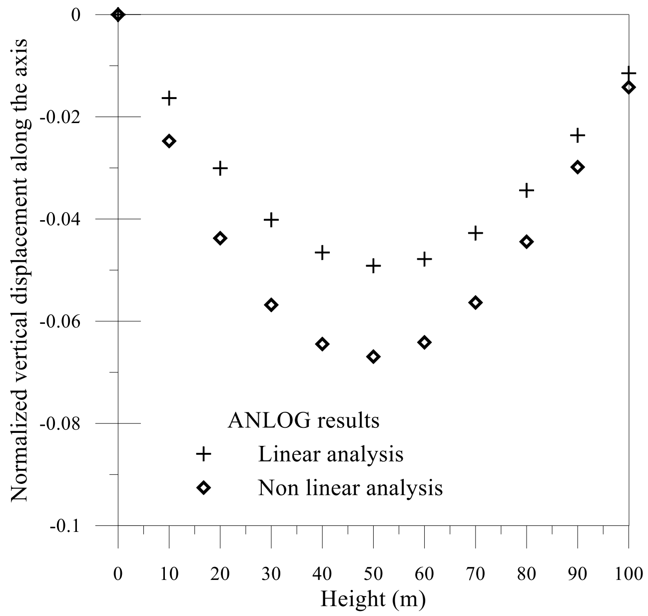


**Figure 12 - Normalized vertical displacement after construction – geometric linear and nonlinear approaches**

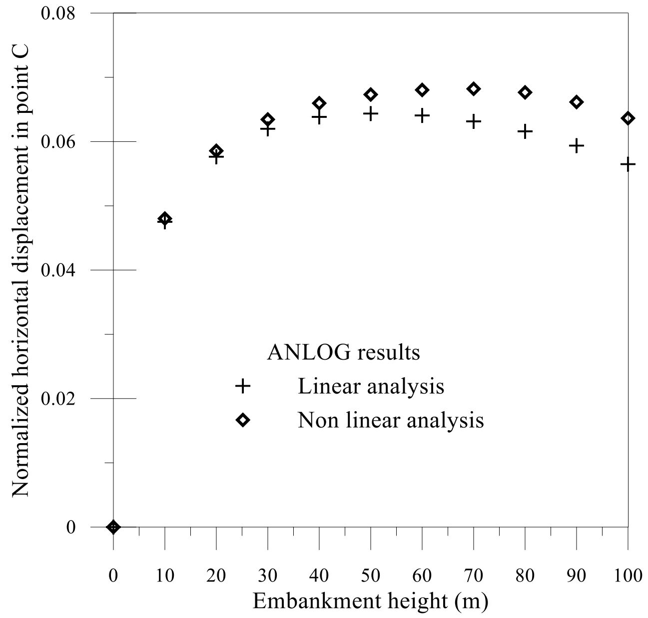


**Figure 13 - Normalized horizontal displacement at point c during construction – geometric linear and nonlinear approaches**

Figure 15 shows horizontal normalized (u/H) displacements and vertical normalized (v/H) displacements in point b' at the moment when b' was on edge of the crest. During the process of construction b' is getting on the slope side. It can be observed that lower horizontal layers have positive displacement in point b' till height of 70, for this geometry of embankment. Observing vertical displacement can be seen that the biggest displacement is for the height of 70 m, when the horizontal is the smallest. Nonlinear analysis shows bigger displacement during the construction process in horizontal and vertical direction.

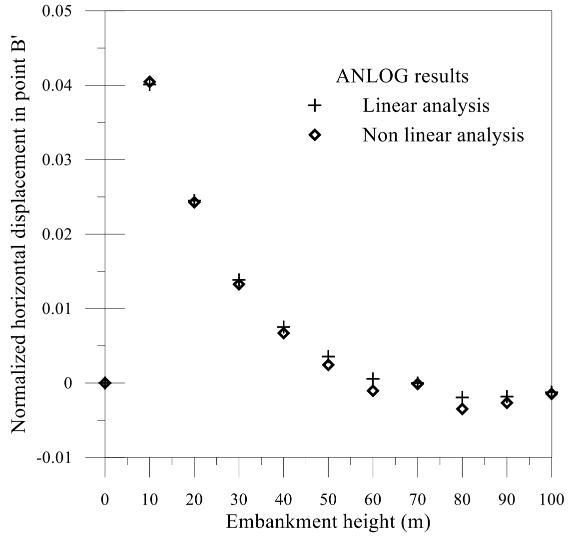


a) Point b' horizontal displacement in construction

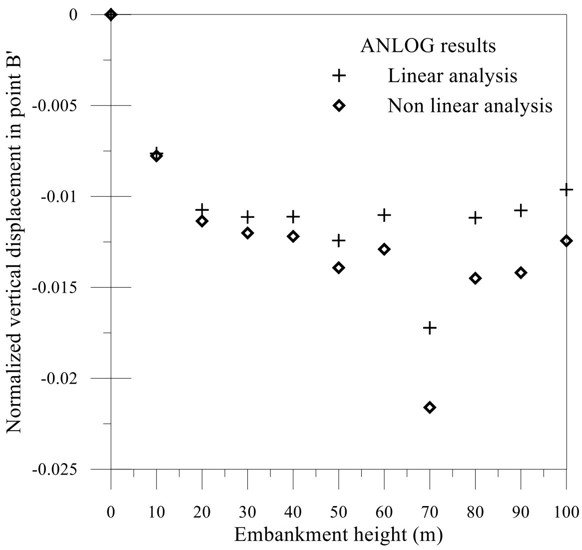


a) Point b' vertical displacement in construction

**Figure 15 - Numerical embankment's movement – geometric linear and nonlinear approaches**

# 4 CONCLUSION

This work presented the total Lagrangian displacement based formulation of finite element method which was implemented into ANLOG. The examples presented revels a good agreement with results from literature. It was shown small difference in results obtained with elements Q4 and Q8 for problem which does not consider body force, as was expected. In nonlinear analysis modified Newton-Raphson process was very efficient with good answers obtained with small amount of iterations.

Examples regarding embankment problem, which takes into account the body force, showed that the influence of geometric nonlinearity increases with the embankment height. Also, the embankment construction process affects the final displacements..

# ACKNOWLEDGEMENTS

The authors are thankful to CAPES, CNPq, FAPEMIG, Fundação Gorceix, PROPEC/UFOP, PPGEM/UFOP and PROPP/UFOP for the support in developing this research.

# REFERENCES

Armond, D. M., Nogueira, C.L, 2013. *Análise via MEF de problemas de fluxo em meio poroso não saturado*. In: XXI SEIC - Seminário de Iniciação Científica da UFOP, Ouro Preto.

Bathe, K. J., 1996. *Finite Element Procedures*. New Jersey, Prentice-Hall.

Battini, JM., 2008. A non-linear corotational 4-node plane element. *Mechanics Research Communications*; vol. 35, pp. 408–413

Belytschko, T., Liu, W.K., Moran, B., Elkhodary, K.I., 2014. *Nonlinear finite elements for continua and structures* Second edition, John Wiley and Sons

Cook, R.D., Malkus, D.S., Plesha, M.E, Witt, R.J., 2002. *Concepts and Applications of Finite Element Analysis*, John Wiley & Sons 4th Edition

Crisfield, M. A., 1991. *Non-linear Finite Element Analysis of Solids and Structures,* John Wiley & Sons

Machado, Jr. J. C., 2000. *Análise de Problemas de Fluxo em Meio Poroso não Saturado pelo Método dos Elementos Finitos*. Masters dissertation, Departamento de Engenharia Civil, PROPEC, UFOP-EM

Mohammadi, S., Taiebat, H. A., 2013. A large deformation analysis for the assessment of failure induced deformations of slopes in strain softening materials, *Computers and Geotechnics* vol. 49 pp. 279–288

Moormann, C., Fatemizadeh, S., Aschrafi, J., 2015. Comparison of advanced numerical methods for geomechanical problems with large deformations, *Proceedings of the XVI ECSMGE Geotechnical Engineering for Infrastructure and Development*

Nogueira, C. L., 1998. *Análise Não Linear de Escavações e Aterros*. PhD thesis, Curso de Pós-Graduação em Engenharia da Pontifícia Universidade Católica do Rio de Janeiro PUC/Rio.

Nogueira, C. L., 2010. *Manual de Utilização do ANLOG*

Pinto, M.A.F., 2004. *Análise numérica via MEF de problemas de adensamento devido à variação do nível d`água*. Masters dissertation, Departamento de Engenharia Civil, PROPEC, UFOP-EM, 128p.

Rupert, M., 2017. *Geometric nonlinear analysis of static geomechanical problem by FEM*, Phd qualification exam, PROPEC/EM/UFOP

Silva, M.A.B., 2005. *Modelo Computacional Tridimensional pelo Método dos Elementos Finitos para Solução de Problemas Geotécnicas*. Masters dissertation, Programa de Pós-graduação em Engenharia Civil - UFV

Silveira, R.A.M, Nogueira, C.L., Gonçalves, P.B., 2013. A numerical approach for equilibrium and stability analysis of slender arches and rings under contact constraints, *International Journal of Solids and Structures* vol.50, pp.147–159

Silveira, R.A.M., Maciel, F.V., Silva, A.R.D. Machado, F.C.S., Nogueira, C.L., 2015. Nonlinear equilibrium and stability analysis of axially loaded piles under bilateral contact constraints, *Latin American Journal of Solids and Structures*, vol 12, pp. 250-270

Simão, J.T., 2014. *Um modelo numérico para análise elastoplástica de maciços rochosos com base no critério de ruptura de Hoek-Brown*. Masters dissertation, PPGEM/EM/UFOP

Timoshenko, S.P., Gere, J.M., 1991. *Mechanics of Materials*, Springer Science + Business Media Dordrecht Third SI edition published in the UK

Valverde, N.N. (2010). *Análise Elasto-plástica 3D de fundações superficiais e aterros pelo Método dos Elementos Finitos*. Masters dissertation , PUC Rio/UFOP

Zienkiewicz O., Taylor R. (2000). *The Finite Element Method: Its Basis and Fundamentals,* Butterworth-Heinemann 5th edition

Zornberg J.G. (1989), *Análise por elementos finitos do comportamento de escavações utilizando um modelo elasto-plástic*. Masters dissertation, PUC-Rio, Rio de Janeiro.